Inorganic Chemistry

Article

Syntheses and Unusual Segregated−Alternated Hybrid Stacking Structure of Hydrogen-Bonded Charge-Transfer Complexes Composed of Bis[2,3-pyridinedithiolate]metal Complexes

Sota Shibahara,*,† Hiroshi Kitagawa,*,‡,|| Yoshiki Ozawa,‡ Koshiro Toriumi,‡ Takashi Kubo,§ and Kazuhiro Nakasuji*,§

Department of Chemistry, Faculty of Science, Kyushu University, Hakozaki 6-10-1, Higashi-ku, Fukuoka 812-8581, Japan, Department of Chemistry, Graduate School of Science, Osaka University, Toyonaka, Osaka 560-0043, Japan, Department of Material Science, Graduate School of Material Science, University of Hyogo, Ako-gun, Hyogo 678-1297, Japan, and JST, CREST, 4-1-8 Hon-chou, Kawaguchi, Saitama 332-0012, Japan

We report the syntheses of new planar electron donor inorganic molecules [bis(2,3-pyridinedithiolate)metal(II)]; [M^{II}(Hpydt)$_2$] (M = Ni(**1**), Pd(**2**), Pt(**3**)) and their anions; [M^{II}(pydt)$_2$]$^{2-}$ (M = Ni(**4**), Pd(**5**)), which are equipped with both a highly lying highest occupied molecular orbital (HOMO) perpendicular to the plane and hydrogen-bonding capability in the plane. In addition, we present two novel hydrogen-bonded charge-transfer (HBCT) complexes, [M(Hpydt)$_2$]TCNQ (M = Ni, Pd), with 7,7,8,8-tetracyanoquinodimethane (TCNQ). All the neutral and ionic inorganic molecules and the HBCT complexes were successfully characterized by single-crystal X-ray crystallography. The HBCT complexes show an unusual segregated−alternated hybrid stacking structure in which each component interacts parallel to the stacks with neighboring donors and acceptors. Furthermore, the structural network is expanded as a result of a one-dimensional hydrogen-bonding chain formed between donors and acceptors perpendicular to the stacking direction. The theoretical electronic structures of the HBCT complexes are also reported.

Introduction

To date, there has been much development in the design of versatile materials comprising electron donors and acceptors for molecular electronics. In this realm of the study of their charge-transfer complexes (CT) and radical cation salts, a whole gamut of molecular metals[1] and molecular superconductors[2] has been discovered. The majority of the CT complexes are composed of π-conjugated organic molecules with a planar geometry. However, the use of transition-metal complexes as building blocks of the CT complex is revolutionary, and consequently, there is considerable interest in recent years for stabilizing the CT state by utilizing d-orbitals.[3] In CT complexes, one of the most important factors required for achieving the desired physical

* To whom correspondence should be addressed. E-mail: sota-s.scc@mbox.nc.kyushu-u.ac.jp (S.S.), hiroshiscc@mbox.nc.kyushu-u.ac.jp (H.K.), nakasuji@chem.sci.osaka-u.ac.jp (K.N.).
† Department of Chemistry, Kyushu University.
‡ Department of Material Science, University of Hyogo.
§ Department of Chemistry, Osaka University.
|| JST, CREST.

(1) (a) Ferraris, J.; Cowan, D. O.; Walatka, V.; Perlstein, J. H. *J. Am. Chem. Soc.* **1973**, *95*, 948−949. (b) Horiuchi, S.; Yamochi, H.; Saito, G.; Sakaguchi, K;, Kusunoki, M. *J. Am. Chem. Soc.* **1996**, *118*, 8604−8622. (c) Hünig, S. *J. Mater. Chem.* **1995**, *5*, 1469−1479. (d) Farges, J. P. *Organic Conductors*; Marcel Dekker: New York, 1994.
(2) (a) Jérome, D.; Mazaud, A.; Ribault, M.; Bechgaard, K. *J. Phys. Lett.* **1980**, *41*, 95−98. (b) Saito, G.; Yamochi, H.; Nakamura, T.; Komatsu, T.; Inoue, T.; Ito, H.; Ishiguro, T.; Kusunoki, M.; Sakaguchi, K.; Mori, T. *Synth. Met.* **1993**, *56*, 2883−2890. (c) Hebard, A. F; Rosseinsky, M. J.; Haddon, R. C.; Murphy, D. W.; Glarum, S. H.; Palstra, T. T. M.; Ramirez, A. P.; Kortan, A. R. *Nature* **1991**, *350*, 600−601.

(3) (a) Kato, R. *Chem. Rev.* **2004**, *104*, 5319−5346. (b) Tanaka, H; Okano, Y.; Kobayashi, H.; Suzuki, W.; Kobayashi, A. *Science* **2001**, *291*, 285−287. (c) Ribas, X.; Sironi, A.; Masciocchi, N.; Lopes, E. B.; Almeida, M.; Veciana, J.; Rovira, C. *Inorg. Chem.* **2005**, *44*, 2358−2366. (d) Bousseau, M.; Valade, L.; Legros, J-P.; Cassoux, P.; Garbauskas, M.; Interrante, V. L. *J. Am. Chem. Soc.* **1986**, *108*, 1908−1916. (e) Nishijo, J.; Ogura, E.; Yamaura, J.; Miyazaki, A.; Enoki, T.; Takano, T.; Kuwatani, Y.; Iyoda, M. *Solid State Commun.* **2000**, *116*, 661−664. (f) Diel, B. N.; Inabe, T.; Lyding, J. W.; Schoch, K. F., Jr.; Kannewurf, C. R.; Marks, T. J. *J. Am. Chem. Soc.* **1983**, *105*, 1551−1567. (g) Faulmann, C.; Errami, A.; Donnadieu, B.; Malfant, I; Legros, J. P.; Cassoux, P.; Rovira, C.; Canadell, E. *Inorg. Chem.* **1996**, *35*, 3856−3873. (h) Rodrigues, J. V.; Santos, I. C.; Gama, V.; Henriques, R. T.; Waerenborgh, J. C.; Duarte, M. T.; Almeida, M. *J. Chem. Soc., Dalton Trans.* **1994**, 2655−2660. (i) Pullen, A. E.; Faulmann, C.; Pokhodnya, K. I.; Cassoux, P.; Tokumoto, M. *Inorg. Chem.* **1998**, *37*, 6714−6720. (j) Wang, G.; Slebodnick, C.; Butcher, R. J.; Tam, M. C.; Crawford, T. D.; Yee, G. T. *J. Am. Chem. Soc.* **2004**, *126*, 16890−16895.

Scheme 1. Synthesis of Metal Complexes **1**−**3** and Dianion Salts **4**−**6**[a]
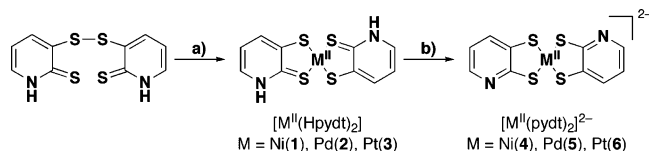
[a] Conditions: (a) [NiCl₂]6H₂O, PdCl₂, or K₂PtCl₄, 10% NaOH aq and (b) 1 N NaOH aq, Et₄NBr (for **4**); 1 N NaOH aq/MeOH, Bu₄NBr (for **5**).

properties is the direct control of the arrangements of the molecules in the crystal. A common design approach is the use of noncovalent interactions within van der Waals distances, such as S···S contacts in the tetrathiafulvalene (TTF) chemistry,[4] while for π−d interactions between organic cations and inorganic magnetic anions, chalcogen···halogen contacts are very effective.[5] An introduction of hydrogen-bonding capability to CT complexes has attracted growing attention for constructing a controlled electronic conductive path.[6] Creation of new electron donor molecules with hydrogen-bonding capability has significance from such a standpoint.

Herein, we report the synthesis and characterization of three new neutral metal complexes, bis(2,3-pyridinedithiolate)metal(II) [M^{II}(Hpydt)₂] (M = Ni(**1**), Pd(**2**), Pt(**3**)), having both electron donor and hydrogen-bonding capabilities, and their deprotonated anion species **4**−**6** (see Scheme 1). The key features of **1**−**3** are the following: (1) several possible intermolecular interactions such as π···π, M···M, M···S, and S···S contacts are expected, and (2) the ligand including a thioamide framework can form hydrogen bonds with many acceptors. We also report the physical properties of two novel HBCT complexes composed of [M(Hpydt)₂] and TCNQ.

Experimental Section

Materials and Methods. All experiments dealing with moisture- or air-sensitive compounds were performed in anhydrous solvents under an argon atmosphere in well-dried glassware. Solvents were dried and distilled according to standard procedures. Infrared spectra of the complexes as powder sample using Nujol technique were recorded on a ThermoNicolet NEXUS 670 Fourier transform infrared (FT-IR) spectrometer. Electronic spectra were measured by transmission through solutions or KBr pellets using a JASCO V-570 spectrophotometer. Raman spectra were recorded on a JASCO NRS-1000 single monochromator with Kaiser Optical Systems Holographic supernotch filter using a microscope. A Showa Optranics GLG5601 He−Ne⁺ laser provided the exciting line (632.8 nm). Detection of the scattered radiation was made by a cooled Princeton Instruments LN/CCD camera system with an operating temperature of 153 K. Wavenumber calibration was made on the basis of the Raman spectrum of silicon and the emission lines of a Ne lamp. Cyclic voltammetric measurements were performed with an ALS-612A electrochemical analyzer using a glassy carbon working electrode, a Pt counter electrode, and a Ag/AgNO₃ reference electrode in dimethylformamide (DMF) (for **1**−**5**) containing 0.1 M Bu₄NClO₄ as the supporting electrolyte in a scan rate of 100 mV/s. The Fc/Fc⁺ couple was used as an internal standard.

Synthesis of Ni(Hpydt)₂ (1·2DMF). The mixture of 3,3′-dithio-bis[pyridine-2(1H)-thione][7] (1.10 g, 3.87 mmol) and nickel chloride·hexahydrate (0.38 g, 1.60 mmol) in 10% NaOH aq (31.6 mL) was refluxed for 12 h. The solution was acidified with 1 M HCl aq and the precipitate was then collected by filtration. Recrystallization from DMF gave red prismatic crystals. Yield 0.70 g (90%).

1·2DMF: mp > 300 °C, IR (Nujol, cm⁻¹) 654, 676, 766, 1037, 1058, 1134, 1295, 1326, 1381, 1425, 1497, 1640, 2023, ca. 2600 (broad), 3075. UV−vis−NIR (in DMF; nm) λ_{max} = 302 (ϵ = 21 700), 534 (ϵ = 5800); Anal. Found: C, 39.24; H, 4.55; N, 11.44. Calcd. for C₁₆H₂₂N₄O₂NiS₄: C, 39.27; H, 4.53; N, 11.45%.

Synthesis of Pd(Hpydt)₂ (2·2DMF). The mixture of bis-3,3′-dithio[pyridine-2(1H)-thione] (1.0 g, 3.52 mmol) and palladium chloride (0.50 g, 2.82 mmol) in 10% NaOH aq (28.7 mL) was refluxed for 12 h. The solution was acidified with 1 M HCl aq and the precipitate was then collected by filtration. Recrystallization from DMF gave orange prismatic crystals. Yield 1.22 g (81%).

2·2DMF: mp > 300 °C, IR (Nujol, cm⁻¹) 649, 675, 768, 1037, 1057, 1132, 1287, 1329, 1382, 1423, 1498, 1641, 2027, ca. 2600 (broad), 3075; UV−vis−NIR (in DMF; nm) λ_{max} = 268 (ϵ = 40 400), 474 (ϵ = 10000); Anal. Found: C, 35.78; H, 4.18; N, 10.51. Calcd. for C₁₆H₂₂N₄O₂PdS₄: C, 35.78; H, 4.13; N, 10.43%.

Synthesis of Pt(Hpydt)₂ (3·2DMF). The mixture of bis-3,3′-dithio[pyridine-2(1H)-thione] (0.35 g, 1.23 mmol) and potassium tetrachloroplatinate (0.43 g, 1.04 mmol) in 10% NaOH aq (10.0 mL) was refluxed for 7 h. The solution was acidified with 1 M HCl aq and the precipitate was then collected by filtration. Recrystallization from DMF gave red prismatic crystals. Yield 0.28 g (43%).

3·2DMF: mp > 300 °C, IR (Nujol, cm⁻¹) 650, 675, 767, 1037, 1058, 1132, 1290, 1329, 1381, 1423, 1498, 1641, 2020, ca. 2600 (broad), 3076; UV−vis−NIR (in DMF; nm) λ_{max} = 285 (ϵ = 16 100), 542 (ϵ = 3100); Anal. Found: C, 30.72; H, 3.49; N, 8.93. Calcd. for C₁₆H₂₂N₄O₂PtS₄: C, 30.71; H, 3.54; N, 8.95%.

Synthesis of 2(Et₄N)⁺·Ni(pydt)₂²⁻·2H₂O (4·2(Et₄N)⁺·2H₂O). To a solution of **1**·2DMF (100 mg, 0.20 mmol) in 1 M NaOH aq (1.0 mL) was added an aqueous solution of Et₄NBr (79 mg, 0.38 mmol). The mixture was allowed to stand at room temperature to give red platelet crystal. Yield 87 mg (68%).

4·2(Et₄N)⁺·2H₂O: mp 185−186 °C, IR (Nujol, cm⁻¹) 663, 785, 1033, 1128, 1359, 1392, 1483, 1548, 3003, 3473; UV−vis−NIR (in DMF; nm) λ_{max} = 308 (ϵ = 36 200), 445 (ϵ = 9100); Anal.

(4) (a) Foumigué, M.; Batail, P. *Chem. Rev.* **2004**, *104*, 5379−5418. (b) Morita, Y.; Murata, T.; Fukui, K.; Yamada, S.; Sato, K.; Shiomi, D.; Takui, T.; Kitagawa, H.; Yamochi, H.; Saito, G.; Nakasuji, K. *J. Org. Chem.* **2005**, *70*, 2739−2744. (c) Morita, Y.; Miyazaki, E.; Umemoto, Y.; Fukui, K.; Nakasuji, K. *J. Org. Chem.* **2006**, *71*, 5631−5637.

(5) Uji, S.; Shinagawa, H.; Terashima, T.; Yakabe, T.; Terai, Y.; Tokumoto, M.; Kobayashi, A.; Tanaka, H.; Kobayashi, H. *Nature* **2001**, *410*, 908−910.

(6) (a) Murata, T.; Morita, Y.; Fukui, K.; Sato, K.; Shiomi, D.; Takui, T.; Maesato, M.; Yamochi, H.; Saito, G.; Nakasuji, K. *Angew. Chem., Int. Ed.* **2004**, *43*, 6344−6346. (b) Itoh, T.; Toyoda, J.; Tadokoro, M.; Kitagawa, H.; Mitani, T.; Nakasuji, K. *Chem. Lett.* **1995**, 41−42. (c) Martin, L.; Turner, S. S.; Day, P.; Guionneau, P.; Howard, J. K. A.; Hibbs, D. E.; Light, M. E.; Hursthouse, M. B.; Uruichi, M.; Yakushi, K. *Inorg. Chem.* **2001**, *40*, 1363−1371. (d) Ribera, E.; Veciana, J.; Molins, E.; Mata, I.; Wurst, K.; Rovira, C. *Eur. J. Org. Chem.* **2000**, 2867−2875. (e) Zaman, Md. B.; Toyoda, J.; Morita, Y;, Nakamura, S.; Yamochi, H.; Saito, G.; Nishimura, K.; Yoneyama, N.; Enoki, T.; Nakasuji, K. *J. Mater. Chem.* **2001**, *11*, 2211−2215. (f) Nishimura, K.; Kondo, T.; Drozdova, O. O.; Yamochi, H.; Saito, G. *J. Mater. Chem.* **2000**, *10*, 911−919. (g) Morita, Y.; Maki, S.; Ohmoto, M.; Kitagawa, H.; Okubo, T.; Mitani, T.; Nakasuji, K. *Org. Lett.* **2002**, *4*, 2185−2188.

(7) Edinberry, M. N.; Gymer, G. E.; Jevons, S. U.K. Patent Application GB, 2053189A, 1981.

Table 1. Crystallographic Data for **1**−**3** and Dianion Salts **4** and **5**

compounds	**1·2DMF**	**2·2DMF**	**3·2DMF**	**4·2(Et₄N)⁺·2H₂O**	**5·2(Bu₄N)⁺**
formula	$C_{16}H_{22}N_4O_2NiS_4$	$C_{16}H_{22}N_4O_2PdS_4$	$C_{16}H_{22}N_4O_2PtS_4$	$C_{26}H_{48}N_4O_2NiS_4$	$C_{42}H_{78}N_4PdS_4$
fw	489.32	537.02	625.71	635.63	873.75
color and habit	red, prism	orange, prism	red, prism	red, block	orange, prism
cryst. system	monoclinic	monoclinic	monoclinic	orthorhombic	monoclinic
space group	$P2_1/c$ (No. 14)	$P2_1/c$ (No. 14)	$P2_1/c$ (No. 14)	$Pbcn$ (No. 60)	$P2_1/c$ (No. 14)
a/Å	7.6204 (4)	7.593 (4)	7.636 (7)	30.74 (1)	9.432 (1)
b/Å	14.3138 (5)	14.365 (5)	14.37 (2)	14.534 (1)	14.584 (2)
c/Å	9.7129 (4)	9.764 (5)	9.695 (9)	14.246 (7)	16.973 (3)
β/deg	100.477 (2)	98.74 (2)	97.96 (9)	90.0	95.846 (8)
V/Å³	1041.80 (7)	1052.6 (9)	1041.80 (7)	6362 (6)	2322.5 (6)
Z	2	2	2	8	2
T/K	200	200	200	296	200
μ (Mo Kα) (cm⁻¹)	1.351	1.298	7.049	0.902	1.249
$D_{calc.}$ (g cm⁻³)	1.56	1.694	1.972	1.327	0.611
reflcns. measd.	9885	8196	10357	10130	23496
reflcns. used	2115	2117	2009	4154	3282
params.	158	168	168	355	280
R1, wR2 [$I > 2\sigma(I)$]	0.025, 0.064	0.032, 0.076	0.032, 0.076	0.050, 0.167	0.027, 0.024
GOF on F^2	1.027	1.048	0.985	1.012	1.069

Found: C, 49.08; H, 7.80; N, 8.85. Calcd. for $C_{26}H_{46}N_4O_2NiS_4$: C, 48.97; H, 7.90; N, 8.79%.

Synthesis of 2(Bu₄N)⁺·Pd(pydt)₂²⁻ (5·2(Bu₄N)⁺). To a solution of **2·2DMF** (50 mg, 0.09 mmol) in 1 N NaOH aq (0.5 mL) was added a MeOH solution (0.7 mL) of Bu₄NBr (57 mg, 0.18 mmol). The mixture was allowed to stand at 4 °C to give red platelet crystal. Yield 61 mg (75%).

5·2(Bu₄N)⁺: mp 189−190 °C, IR (Nujol, cm⁻¹) 652, 737, 774, 881, 1030, 1128, 1219, 1236, 1363, 1381, 1481, 1546, 3078; UV−vis−NIR (in DMF; nm) $\lambda_{max} = 269$ ($\epsilon = 44\,900$), 406 ($\epsilon = 12\,700$); Anal. Found: C, 57.50; H, 8.61; N, 6.24. Calcd. for $C_{42}H_{79}N_4$-PdS₄: C, 57.73; H, 9.00; N, 6.41%.

Synthesis of 1·TCNQ. X-ray quality single crystals were prepared by a conventional diffusion method using an H-shaped cell. Each arm of the cell was charged with **1·2DMF** (5.0 mg, 0.01 mmol) and TCNQ (4.0 mg, 0.02 mmol), and 15 mL mixture of acetone:acetonitrile = 4:1 was poured onto the solid carefully at 60 °C. After slowly cooling to 30 °C, black prismatic crystals were collected by filtration and were washed with acetonitrile. Yield 4.1 mg (75%).

1·TCNQ: mp > 300 °C, IR (Nujol, cm⁻¹) 1583, 1558, 2154, 2173, 2213, 3104, 3138, 3227; Anal. Found: C, 48.22; H, 2.25; N, 15.36. Calcd. for $C_{16}H_{22}N_4O_2NiS_4$: C, 48.28; H, 2.21; N, 15.35%.

Synthesis of 2·TCNQ. X-ray quality single crystals were prepared by a conventional diffusion method using an H-shaped cell. Each arm of the cell was charged with **2·2DMF** (50 mg, 0.09 mmol) and TCNQ (110 mg, 0.22 mmol), and 50 mL of acetonitrile was poured onto the solid carefully at 60 °C. The mixture was allowed to stand at 60 °C for 30 days to give black prismatic crystals. Yield 30.6 mg (57%).

2·TCNQ: mp > 300 °C, IR (Nujol, cm⁻¹) 1583, 1557, 2151, 2171, 2216, 3104, 3231; Anal. Found: C, 44.18; H, 1.96; N, 14.12. Calcd. for $C_{12}H_{22}N_6PdS_4$: C, 44.41; H, 2.03; N, 14.12%.

X-ray Crystallography. Data collections were performed on a Rigaku RAXIS-RAPID imaging-plate diffractometer (Mo Kα, $\lambda = 0.71069$ Å) for **1·2DMF**, **2·2DMF**, **3·2DMF**, **5·2(Bu₄N)⁺**, and **2·TCNQ** and on a Rigaku AFC5R (Mo Kα, $\lambda = 0.71069$ Å) for **4·2(Et₄N)⁺·2H₂O**. The structures were solved with direct methods and were refined on F^2 by full-matrix least squares (SHELX-97). All non-hydrogen atoms were refined anisotropically. Hydrogen atoms were placed in their calculated positions. Crystallographic details are summarized in Tables 1 and 5. For **1·TCNQ**, data were collected at 298 K using synchrotron radiation (22.18 keV ($\lambda =$

Table 2. Selected Bond Lengths (Å) and Angles (deg) for **1**−**3** and Dianion Salts **4** and **5**

	1·2DMF	**2·2DMF**	**3·2DMF**	**4²⁻·2(NEt)⁺·H₂O**	**5²⁻·2(NBu)⁺**
M−S(1)	2.170	2.298	2.296	2.192	2.303
M−S(2)	2.177	2.299	2.298	2.178	2.287
M−S(3)				2.193	
M−S(4)				2.165	
S(1)−C(1)	1.723	1.734	1.736	1.741	1.753
S(2)−C(2)	1.734	1.743	1.740	1.763	1.747
S(3)−C(6)				1.730	
S(4)−C(7)				1.750	
C(1)−N(1)	1.346	1.354	1.352	1.351	1.342
C(5)−N(1)	1.350	1.348	1.355	1.328	1.333
C(6)−N(2)				1.359	
C(10)−N(2)				1.329	
C(1)−C(2)	1.409	1.414	1.410	1.405	1.416
C(2)−C(3)	1.386	1.388	1.392	1.361	1.377
C(3)−C(4)	1.387	1.395	1.378	1.388	1.375
C(4)−C(5)	1.365	1.369	1.368	1.360	1.357
C(6)−C(7)				1.413	
C(7)−C(8)				1.377	
C(8)−C(9)				1.377	
C(9)−C(10)				1.358	
N(1)−H···O	2.687	2.697	2.691		
S(1)−M−S(2)	92.03	89.55	89.43	91.88	89.3
S(3)−M−S(4)				91.67	

0.5592 Å) and the MAC Science low-temperature vacuum X-ray camera equipped with an imaging plate (IP) area detector at the BL02B1 beamline of the SPring-8 facility. A crystal with dimensions $0.07 \times 0.04 \times 0.01$ mm mounted on carbon fibers was used. The frames were indexed, and the reflections were integrated using DENZO and were subsequently scaled using SCALEPACK.[23a] An empirical correction for absorption anisotropy was applied to all intensity data by using of PLATON-MULABS.[23b] The structure was solved by direct methods (SHELXS-97)[24a] and was refined by full-matrix least-squares techniques on F^2 (SHELXL-97).[24a] All non-hydrogen atoms were placed at their idealized positions and were not refined. All calculations were performed with the teXsan crystallographic software package.[24b]

Computational Method. All the density funcitonal theory (DFT) calculations of the metal complexes **1**−**3** were done at the RB3LYP/LANL2DZ level using the Gaussian 03 program.[25] The lowest excited states of the closed-shell metal complexes were calculated by the time-dependent DFT (TD−DFT) method. The X-ray crystallographic data in CIF files were used for the atom positions of the metal complexes. The band calculations for **1·TCNQ** and **2·TCNQ** were performed using YAeHMOP package in the X-ray
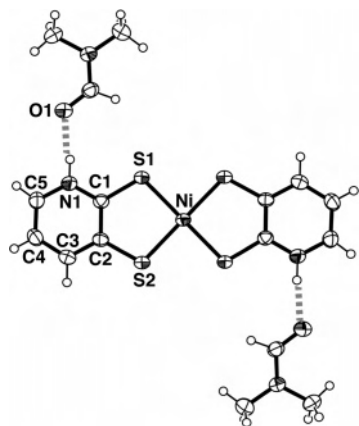
Figure 1. ORTEP drawing of **1·2DMF** with thermal ellipsoids drawn at 50% probability. The dotted line represents a hydrogen bond.

[M(Hpdt)₂], (M = Ni, Pd, Pt)
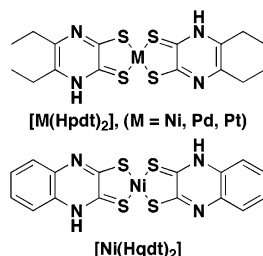
[Ni(Hqdt)₂]

Figure 2. Molecular structures of [M(Hpdt)₂] and [Ni(Hqdt)₂].
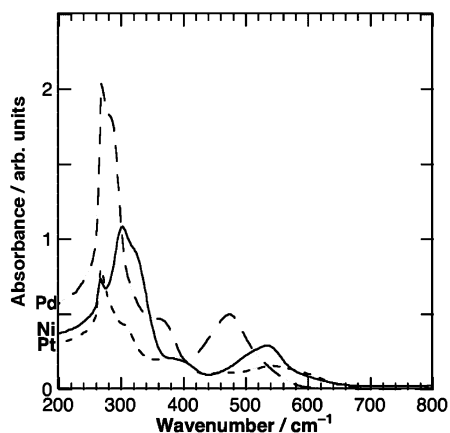
Figure 3. Electronic absorption spectra for **1−3** in DMF (0.05 mM solutions). Filled line: Ni complex, dashed: Pd complex, dotted line: Pt complex.

Table 3. Electronic Transition Data and the Intense Peaks Predicted by TD−DFT Calculation for **1−3**

	λ_{max} (DMF, nm)	ϵ (M⁻¹ cm⁻¹)	λ_{max} (calc., nm)
1·2DMF	534	5800	508
2·2DMF	474	10 000	523
3·2DMF	542	3100	582

crystallographic geometry. Yet Another Extended Hückel Molecular Orbital Package (YAeHMOP, including bind 3.0 and viewkel 3.0) is freely available on the Internet at http://sourceforge.net/projects/yaehmop/.

Default extended Hückel parameters were employed for all elements in the calculation.

Electrical Conductivity. DC conductivities were measured with a standard quasi-four-probe technique, using gold paint to attach gold wires to the compressed pellet.
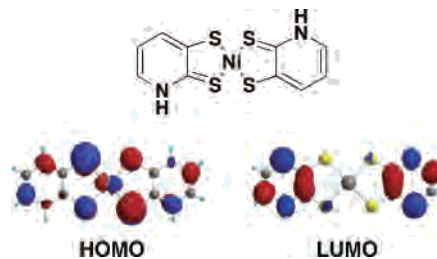
Figure 4. Calculated HOMO (b_g; left) and LUMO (a_u; right) for **1**.

**Table 4.** Redox Potentials of Neutral Species **1−3** and Dianion Species **4** and **5**[c]

	1	**2**	**3**	**4**	**5**
$E_{1/2}^{II/III}$	−0.10		−0.15	−0.83	−0.55
$E_{1/2}^{III/IV}$	+0.18[a]		+0.15[a]	+0.18[a]	+0.13[a]
$E_{1/2}^{II/IV}$		+0.16[a,b]			

[a] E_{pa}. [b] One-step two-electron process. [c] See Exprimental Section for measurement conditions.

Results and Discussion

Syntheses, Crystal Structures, and Physical Properties of 1−3. The precursor, 3,3′-dithio-bis[pyridine-2(*1H*)-thione], was prepared by modifying a synthetic procedure previously reported.[7] Metal complexes **1−3** were synthesized according to the procedure outlined in Scheme 1. Single crystals of the solvated metal complexes **1−3·2DMF** were obtained by recrystallization from *N,N*-dimethylformamide (DMF) along with a few drops of trifluoroacetic acid (TFA). Deprotonation of **1** and **2** with aqueous 1 M NaOH in the presence of quarternary alkyl ammonium salts (R_4N^+ Br⁻; R = ethyl or butyl) gave single crystals of the dianion salts **4**·2($Et_4N)^+$· $2H_2O$ and **5**·2($Bu_4N)^+$, respectively. However, a similar procedure did not result in X-ray quality single crystals including **6** in spite of many attempts. The molecular structure of the metal complexes **1−3·2DMF** and the dianion salts **4**·2($Et_4N)^+$·$2H_2O$ and **5**·2($Bu_4N)^+$ were characterized by single-crystal X-ray crystallography. The crystallographic data of the complexes are summarized in Table 1. The selected bond lengths and angles of **1−3·2DMF**, **4**·2($Et_4N)^+$· $2H_2O$, and **5**·2($Bu_4N)^+$ are given in Table 2. Figure 1 shows the Ortep diagram of the metal complex **1**. The molecular structures are square-planar coordination with trans-configuration of the two ligands. The neutral metal complex **1** forms N−H···O hydrogen bonds with DMF molecules (N1− O1: ca. 2.69 Å). To estimate the oxidation states of the metal ions, the M−S bond lengths and S−M−S angle of complexes **1−3** were compared to those of bis[5,6-diethyl−2,3-pyrazinedithiolate]metal complexes, [M(Hpdt)₂] (M = Ni, Pd, Pt).[8] The molecular structures of [M(Hpdt)₂] are shown in Figure 2. The oxidation states of M ions in [M(Hpdt)₂] were II+. The identical Ni−S distance (2.170(1) and 2.177(1) Å) and the interchelate S−Ni−S angle (92.03(2)°) of the complexes **1** are similar to those (2.168(1), 2.171(1) Å and 92.75(3)°) of [Ni^II(Hpdt)₂]. The X-ray analyses also indicated that the Pd, Pt complexes and Pd dianion have the same square-planar coordination (see CIF file). The M−S distances

(8) Kubo, T.; Ohashi, M.; Miyazaki, K.; Ichimura, A.; Nakasuji, K. *Inorg. Chem.* **2004**, *43*, 7301−7307.
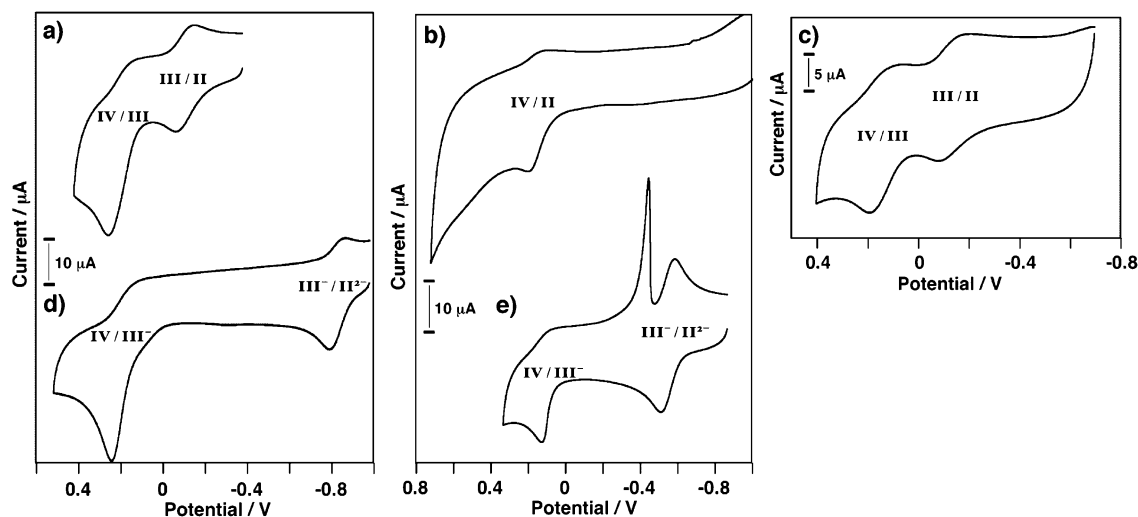
Figure 5. Cyclic voltammograms of (a) neutral species **1**, (b) **2**, (c) **3**, (d) dianion species **4**, and (e) **5** in DMF.
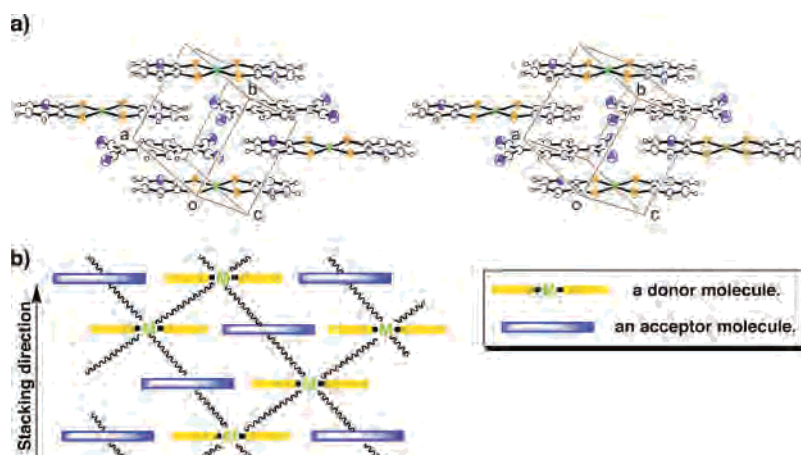
Figure 6. (a) Stereoview of the crystal packing of **1**·TCNQ, showing π-stacking columns between donor−donor, acceptor−acceptor, and donor−acceptor. (b) An illustration for the stacking structure of **1**·TCNQ. The wavy lines denote effective overlaps existing between the molecules.

and S−M−S angles (2.2984(6), 2.2992(6) Å, and 89.55(2)° for **2**; 2.2975(7), 2.2965(8) Å, and 89.43(3)° for **3**) of the complexes **2**−**3** are also similar to those (2.289(1), 2.305(6) Å, and 89.54(2)° for Pd complex; 2.285(2), 2.305(2) Å, and 89.63(7)° for Pt complex) of [M^{II}(Hpdt)$_2$], thus the oxidation states of metal ions in **1**−**3** are considered to be II+.

The oxidation state of Ni in the complex **1**·2DMF can be also estimated by the natural population analysis on the basis of DFT method (RB3LYP/LANL2DZ).[9] The result of the analysis for **1**·2DMF gives 9.05 electrons on 3d-orbital of the Ni atom, which coincides with the value of a Ni ion having a formal d^8 configuration with σ-donation from the ligands to the Ni ion.[9b]

As shown in Table 2, the average C−S bond lengths 1.746 and 1.750 Å in the dianion species **4** and **5** are larger than those (1.729 and 1.739 Å) of neutral species **1** and **2**, respectively. It is well-known in metal bis(dithiolene) systems that C−S bonds of dianion species are longer than those of neutral species. For example, in bis(quinoxaline-2,3-dithio-lato)nickel(II) complexes [Ni(Hqdt)$_2$][10] as shown in Figure 2, the C−S bond lengths of the deprotonated dianion [Ni(qdt)$_2$]$^{2-}$ are 1.78(1) and 1.73(1), while those of the protonated neutral [Ni(Hqdt)$_2$] are 1.703(4) and 1.732(4). The elongations in the C−S bonds are interpreted by the double bond character and decreased as a result of negative charge generated by deprotonation.

To know the electronic structure around highest occupied molecular orbital/lowest unoccupied molecular orbital (HOMO/LUMO) levels, electronic absorption spectra of the metal complexes **1**−**3** in DMF were measured at room temperature. Figure 3 shows the electronic absorption spectra of **1**−**3**. An intense absorption band was observed for each for the metal complex around 500 nm. The absorption maximum (λ_{max}) and molar absorption coefficient (ϵ) are summarized in Table 3. The origin of the intense band was examined by means of time-dependent DFT (TD−DFT) calculations. The result of TD−DFT calculations for the metal complex **1** suggested that the intense band is attributable to the HOMO (b$_g$) → LUMO (a$_u$) transition. As shown in Table 3, the value

(9) (a) Lauterbach, C.; Fabian, J. *Eur. J. Inorg. Chem.* **1999**, 1995−2004. (b) Bachler, V.; Olbrich, G.; Neese, F.; Wieghardt, K. *Inorg. Chem.* **2002**, *41*, 4179−4193.

(10) (a) Pignedoli, A.; Peyronel, G. *Acta Crystallogr., Sect. B* **1977**, *33*, 1439−1443. (b) Pignedoli, A.; Peyronel, G.; Antolini, L. *Acta Crystallogr., Sect. B* **1974**, *30*, 2181−2185.

Table 5. Crystallographic Data for CT Complex of **1**·TCNQ and **2**·TCNQ

compounds	**1**·TCNQ	**2**·TCNQ
formula	$C_{12}H_{22}N_6NiS_4$	$C_{12}H_{22}N_6PdS_4$
fw	547.33	595.02
color and habit	black, prism	black, prism
cryst. system	triclinic	triclinic
space group	P$\bar{1}$ (No. 2)	P$\bar{1}$ (No. 2)
a/Å	7.3730 (4)	7.5745 (3)
B/Å	8.4850 (10)	8.6899 (7)
c/Å	9.8660 (11)	9.9095 (5)
α/deg	70.565 (6)	69.27 (4)
β/deg	80.957 (6)	80.71 (5)
γ/deg	69.641 (6)	68.98 (4)
V/Å^3	545.09 (10)	569.0 (2)
Z	1	1
T/K	293	200
μ (Mo Kα) (cm^{-1})	0.677	1.207
$D_{calc.}$ (g cm^{-3})	1.667	1.736
reflcns. measd.	2906	5624
reflcns. used	2906	2083
params.	151	175
R1, wR2 [$I > 2\sigma(I)$]	0.050, 0.129	0.069, 0.129
GOF on F^2	1.187	1.141

Table 6. Transfer Integrals (in meV) of Donor−Acceptor, Donor−Donor, and Acceptor−Acceptor Overlaps in the HBCT Complexes

	1·TCNQ		**2**·TCNQ	
	HOCO^a	LUCO^b	HOCO^a	LUCO^b
D−A	39	10	24	6
D−D	21		24	
A−A		3		0

^{a} Highest occupied crystal orbital. ^{b} Lowest unoccupied crystal orbital.

Table 7. Comparison of Intramolecular C−C Bond Lengths in TCNQ Moiety in **1**·TCNQ and **2**·TCNQ, Neutral TCNQ^0, and Completely Ionic TCNQ$^{\bullet-}$
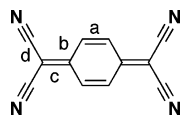
	a/Å	b/Å	c/Å	d/Å
1·TCNQ	1.343	1.426	1.378	1.419
2·TCNQ	1.352	1.456	1.391	1.451
TCNQ$^{0\ 16a}$	1.346	1.431	1.394	1.423
TCNQ$^{\bullet-\ 16b}$	1.373	1.423	1.420	1.416

obtained by the calculation is approximately consistent with the observed one. The HOMO and LUMO for the metal complex **1** are shown in Figure 3. The HOMO is distributed both on metal atom and the ligands, whereas the LUMO is distributed only on the ligands. Hence, the transition can be assigned as MMLL (mixed metal−ligand to ligand) CT.[11] Distributions of HOMO and LUMO for **2** and **3** were also similar to those of **1**. Therefore, it is considered that the intense bands observed for **2** and **3** can be assigned as the HOMO−LUMO transition. The intense bands for metal complexes **1**−**3** give the order of increasing energy as Pt < Ni < Pd, which is inconsistent with the results of the TD−DFT calculations (Pt < Pd < Ni). The observed order of the transition energies was often reported in square-planar

(11) Cocker, T. M.; Bachman, R. E. *Inorg. Chem.* **2001**, *40*, 1550−1556.

d^8 transition-metal complexes.[8,11,12] The observed metal dependence of the HOMO−LUMO transition energy (Pt < Ni < Pd) was discussed mainly from the HOMO level,[11] because the HOMO is delocalized both on the metal and ligands, while the LUMO is localized on the ligands.

To know the electron-donating abilities of the metal complexes, electrochemistry of the neutral and the dianion species was investigated using cyclic voltammetry (CV). The cyclic voltammograms of **1**−**5** are shown in Figure 4. The redox potentials are summarized in Table 4. Two irreversible redox waves were observed in the voltammograms of the neutral species **1** and **3**, presumably caused by deprotonation of the amide moieties in the complexes or by intrinsic instability of highly oxidized species. This phenomenon is often observed for the molecules having dissociative protons, the so-called proton-coupled redox system.[8,13] As shown in Table 4, the first redox potentials of **1** and **3** are −0.10 and −0.15 V, respectively. It indicates that the electron-donating abilities of the complexes are comparable to that of tetrathiafulvalene (TTF).[14] The redox wave (+0.16 V) of **2** showed one-step two-electron process, which is indicative of decreased on-site Coulomb repulsion of mono-oxidized species, compared to **1** or **3**. In the voltammograms of dianion species **4** and **5**, the first redox wave ($E_{1/2}^{II/III}$) is significantly shifted to lower voltage (−0.83 for **4** and −0.55 V for **5**). This finding suggests that deprotonation of the metal complexes drastically increases the electron-donor abilities. The appearance of the sharp reduction wave around −0.45 V in the voltammogram of **5** implies adsorption of salts on the electrode. From the values of the first redox potential for **1**−**3**, it can be concluded that the energy of the HOMO, that is, the electron-donating ability, increases in the order of Pd < Ni < Pt. Additionally, this order is consistent with the metal dependence of the transition energies in the electronic absorption spectra as mentioned above.

Unconventional Segregated−Alternated Hybrid Stacking Structures of 1·TCNQ and 2·TCNQ. To prepare HBCT complexes, the metal complexes **1**−**3** were made to react with TCNQ. Reaction of **1** or **2** with TCNQ using a conventional diffusion method gave black prismatic HBCT crystals. The structures of the HBCT complexes were successfully determined by single-crystal X-ray crystallography. Figure 6a shows a stereoview of the crystal packing of **1**·TCNQ. The stacking structure of **1**·TCNQ is understandably illustrated in Figure 6b. The wavy lines denote effective overlaps existing between the molecules. The crystallographic data are listed in Table 5. The two HBCT complexes have almost the same geometries with the stoichiometry of donor:acceptor = 1:1. However, they display an unusual stacking mode where a donor molecule overlaps other donor molecules as well as acceptor ones. In general, CT complexes can be categorized either as segregated or alternated stacking modes. These HBCT complexes,

(12) Forbes, C. E.; Holm, R. H. *J. Am. Chem. Soc.* **1970**, *92*, 2297−2303.
(13) Haga, M.; Ali, Md. M.; Koseki, S.; Fujimoto, K.; Yoshimura, A.; Nozaki, K.; Ohno, T.; Nakajima, K.; Stufkens, D. *J. Inorg. Chem.* **1996**, *35*, 3335−3347.
(14) The first oxidation potential of TTF was −0.09 V (vs Fc/Fc⁺) in DMF.
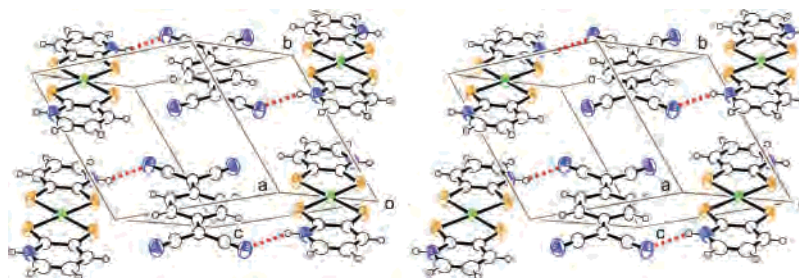
Figure 7. Stereoview of the crystal packing of **1**·TCNQ, showing N−H⋯N hydrogen bonding (red).
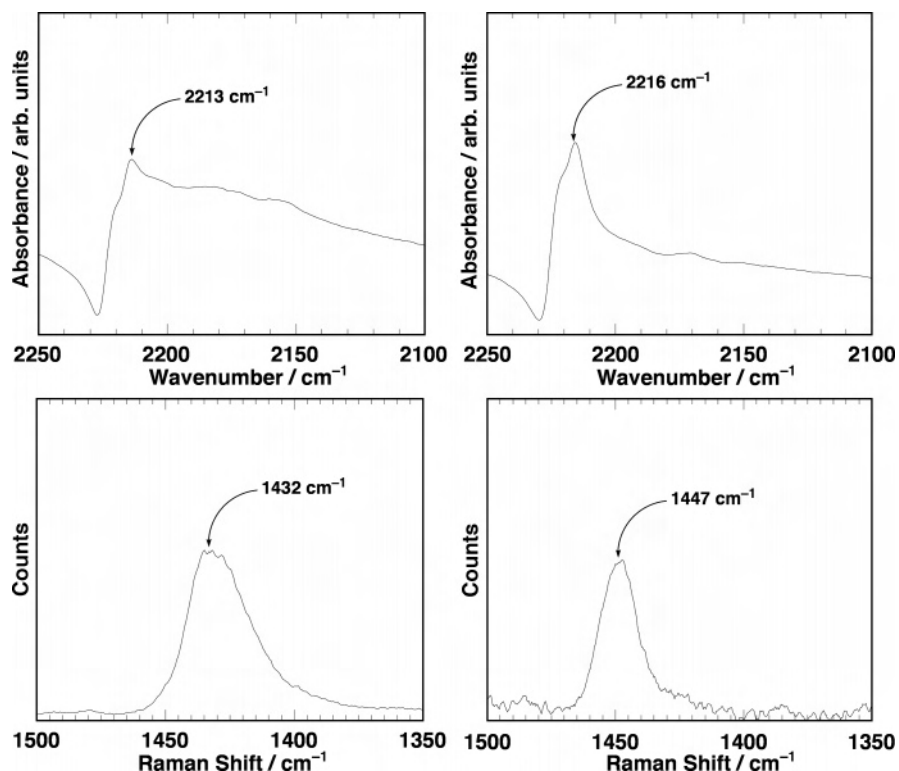
Figure 8. Partial IR spectra of (a) **1**·TCNQ and (b) **2**·TCNQ. C≡N stretching vibration mode (B_{1u}) is observed at 2213 cm^{-1} (for **1**, indicating $\rho = 0.3$) and 2216 cm^{-1} (for **2**, indicating $\rho = 0.2$) in IR spectra. Partial Raman spectra of (c) **1**·TCNQ and (d) **2**·TCNQ. C=C stretching vibration mode (A_g) are observed at 1432 cm^{-1} (for **1**, indicating $\rho = 0.4$) and 1447 cm^{-1} (for **2**, indicating $\rho = 0.1$) in Raman spectra.

however, possess both segregated and alternated stackings, and thus can be categorized into "a segregated−alternated hybrid stacking". The closest interatom distances among each component are the following: for **1**·TCNQ: 3.504 Å (C2−C5 for D−D), 3.394 Å (C1−C8 for D−A), and 3.338 Å (N3−C10 for A−A); for **2**·TCNQ: 3.497 Å (C2−C5 for D−D), 3.443 Å (C1−C8 for D−A), and 3.389 Å (N3−C10 for A−A). The overlap area of the A−A stacking is considerably smaller than that of the D−D and D−A stacking. There are not only $\pi-\pi$ interactions but also $\pi-$d interactions between D−A stacking (Ni1−C10: 3.529 Å for **1**·TCNQ, Pd1−C4: 3.588 Å for **2**·TCNQ). The relationship of the strength for CT interactions among the stackings should be substantially dictated by the interatom distances and overlap areas, because Mulliken reported that CT interaction depends on the interatom distances.[15] Furthermore, the donor and the acceptor are connected through N−H⋯N hydrogen bonds along the $a + c$-axis. Figure 7 shows the
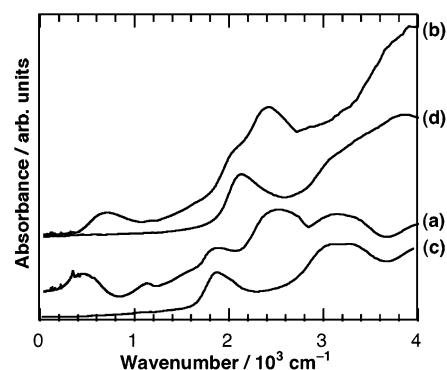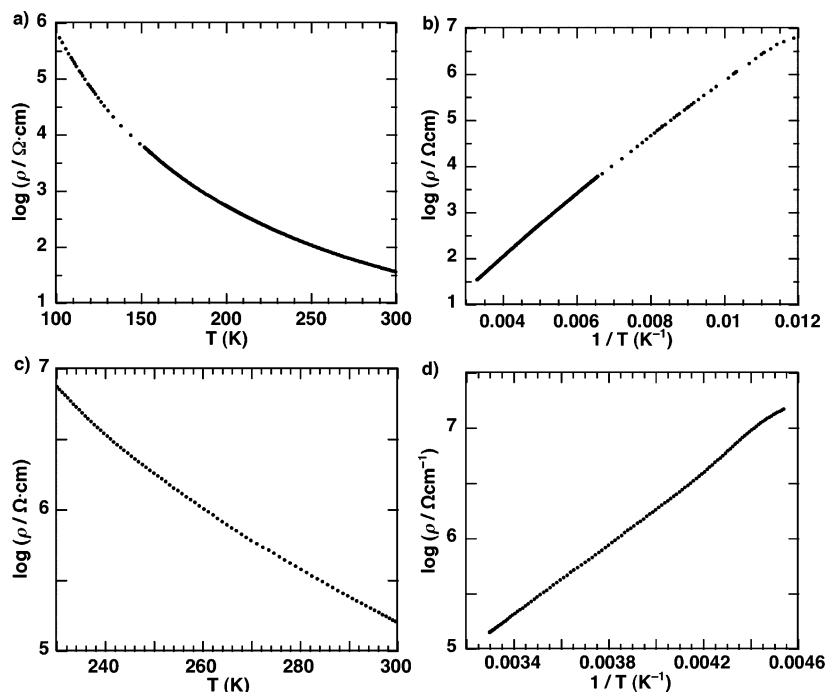
(15) Mulliken, R. S.; Person, W. B. *Annu. Rev. Phys. Chem.* **1962**, *13*, 107−126.

Figure 9. Electronic absorption spectra of (a) **1**·TCNQ, (b) **2**·TCNQ, (c) **1**·2DMF, and (b) **2**·2DMF measured using KBr pellet.

stereoview of the crystal packing of **1**·TCNQ, showing N−H⋯N hydrogen bondings. The hydrogen bond distances (N1−H3⋯N2) of the HBCT complexes are 3.004 Å for **1**·TCNQ and 3.026 Å for **2**·TCNQ. As shown in Figure 7, the structural network is expanded as a result of a one-dimensional hydrogen-bonding chain formed between donors and acceptors perpendicular to the stacking direction.

Figure 10. Temperature dependence of the electrical resistivity of (a) **1·**TCNQ and (c) **2·**TCNQ, measured by the quasi-four-probe method using the compressed pellet. The $1/T$ plot for the values of log ρ. (b) **1·**TCNQ and (d) **2·**TCNQ.

The electronic structure of the unusual stacking of **1·**TCNQ and **2·**TCNQ was investigated using band structure calculations on the basis of the extended Hückel theory. The band dispersion is dominantly extended along the stacking direction and the transfer integrals for the D−A, D−D, and A−A overlaps are summarized in Table 6. The D−D and D−A transfer integrals are comparable for a bandwidth of HOCO (highest occupied crystal orbital), whereas the A−A transfer integrals are quite small and negligible.[16] These results suggest that orbital overlaps through the D−D and D−A stackings may generate a conduction path. To the best of our knowledge, coexistence of D−D and D−A stackings has been found only for two CT complexes, dibenzotetrathiafulvalene−TCNQ (DBTTF−TCNQ) and dibenzotetrathiafulvalene−2,5-difluoro-7,7,8,8-tetracyanoquinodimethane (DBTTF−F₂TCNQ).[17] Hydrogen bonds do not exist in DBTTF−TCNQ and DBTTF−F₂TCNQ. In the case of **1·**TCNQ and **2·**TCNQ, an additional interaction, that is, hydrogen bonds, is utilized for regulating the segregated−alternated hybrid stacking structure. Thus, the HBCT complexes exhibit the unprecedented occurrence of π−π, π−d within the stacks and hydrogen-bond interactions between stacks in the crystal structures.

Ionicity and Electrical Resistivity of 1·TCNQ and 2·TCNQ. Estimating the charge-transfer degree of a CT complex gives much important information about the physical properties. Charge-transfer degree (ionicity: ρ) from an electron donor to an acceptor molecule can be estimated by the ratio of the bond lengths of quinoid moiety in the TCNQ

molecule in its different charge states.[18] Table 7 lists C−C bond lengths of TCNQ in **1·**TCNQ and **2·**TCNQ. The C−C bond lengths of TCNQ⁰ and TCNQ⁻¹, which are exemplified as a standard of neutral and ionic states, are also shown in Table 7. The ionicities of **1·**TCNQ and **2·**TCNQ are ca. 0.4 and 0.1, respectively. The difference of ionicities between **1·**TCNQ and **2·**TCNQ is caused by the energy gap between HOMO of the donor and LUMO of the acceptor.[19] Moreover, IR[20] and Raman[21] spectroscopies are also informative for the ionicity of TCNQ, because the stretching vibration energies $\nu_{C\equiv N}$ and $\nu_{C=C}$ are decreased because of lengthening C≡N and C=C bonds in TCNQ when a neutral state of TCNQ accepts an electron. We performed IR and Raman spectroscopic measurements using the HBCT complexes. The IR spectra around C≡N stretching vibration region of [M(Hpydt)₂]TCNQ are shown in Figure 8. The C≡N stretching vibration modes (B₁ᵤ) of the HBCT complexes were observed at 2213 cm⁻¹ for **1** ($\rho = 0.3$) and 2216 cm⁻¹ for **2** ($\rho = 0.2$) in the IR spectra. The Raman spectra in the C=C stretching vibration region for [M(Hpydt)₂]TCNQ are also shown in Figure 8. The C=C stretching vibration modes (Aᵍ) of the HBCT complexes were observed at 1432 cm⁻¹ for **1** ($\rho = 0.4$) and 1447 cm⁻¹ for **2** ($\rho = 0.1$) in the Raman spectra, which agrees with those obtained from the ratio of bond lengths of TCNQ in the HBCT

(16) For low-dimension conductors, the band width (*W*) is approximately equal to 4 times transfer integrals (4*t*).

(17) Emge, T. J.; Wiygul, F. M.; Chappell, J. S.; Bloch, A. N.; Ferraris, J. P.; Cowan, D. O.; Kistenmacher, T. J. *Mol. Cryst. Liq. Cryst.* **1982**, *87*, 137−161.

(18) (a) Flandrois, S.; Chasseau, D. *Acta Crystallogr., Sect. B* **1977**, *33*, 2744−2750. (b) Kistenmacher, T. J.; Emge, T. J.; Bloch, A. N.; Cowan, D. O. *Acta Crystallogr., Sect. B* **1982**, *38*, 1193−1199.

(19) The first reduction potential of TCNQ was −0.17 V (vs Fc/Fc⁺) in DMF. $\Delta E_{redox} = E_{ox1}$ (donor) − E_{red1} (acceptor) = 0.07 V for **1·**TCNQ and 0.33 V for **2·**TCNQ. HOMO−LUMO gap of the complexes could be roughly estimated with the value of ΔE_{redox}.

(20) Chappell, J. S.; Bloch, A. N.; Bryden, W. A.; Maxfield, M.; Poehler, T. O.; Cowan, D. O. *J. Am. Chem. Soc.* **1981**, *103*, 2442−2443.

(21) Matuzaki, S.; Kuwata, R.; Toyoda, K. *Solid State Commun.* **1980**, *33*, 403−405.

complexes as described above. Definitely, the C=C bond lengths of TCNQ and stretching vibration energy $\nu_{C\equiv N}$ or $\nu_{C=C}$ of **1**·TCNQ and **2**·TCNQ suggested the ionicities of 0.3−0.4 and 0.1−0.2 at ambient condition, respectively.

To investigate the charge-transfer interactions in the HBCT complexes, electronic absorption spectra using the powdered samples in KBr pellets were measured at room temperature. Figure 9 shows the electronic absorption spectra of the HBCT complexes and the donor molecules. The CT bands were observed at 4800 cm^{-1} for **1**·TCNQ and 7200 cm^{-1} for **2**·TCNQ, being assigned to intermolecular excitation of the electron from HOMO of the donor to LUMO of the acceptor. It is reasonable that the CT bands appear in lower-energy region compared to the intramolecular excitation bands (at around 2.0×10^4 cm^{-1}) of each donor molecule. The difference in the transition energies of the two CT bands is assumed to be due to the magnitude in the energy gaps between HOMO of the donor and LUMO of the acceptor[14] and the intermolecular stacking distances between D−A molecules in each CT complex as mentioned above. In CT complexes showing highly conductive behavior, the CT band generally appears at <5000 cm^{-1}.[22]

To reveal the electrical property for the HBCT complexes, electrical resistivities of compressed pellets of **1**·TCNQ and **2**·TCNQ were measured by a quasi-four-probe method. Figure 10 provides a plot of log ρ against T or $1/T$ for the HBCT complexes. Both HBCT complexes showed semi-conducting behavior with a room-temperature resistivity of 3.7×10^1 Ω cm ($E_a = 128$ meV) for **1**·TCNQ and 5.7×10^4 Ω cm ($E_a = 326$ meV) for **2**·TCNQ. The more insulating behavior of **2**·TCNQ would be due to the almost neutral electronic state. These results are consistent with the order of the CT band energy, 4800 cm^{-1} (**1**·TCNQ) < 7200 cm^{-1} (**2**·TCNQ).

Conclusion

We succeeded in the syntheses and characterizations of new metal complexes [M^{II}(Hpydt)$_2$]2DMF (M = Ni, Pd, Pt), which behave as electron donor equipped with hydrogen-bonding ability. Cyclic voltammetry measurements for each complex suggest that the electron-donating abilities of **1** and **3** are comparable to that of TTF. The hydrogen-bonded charge-transfer complexes composed of **1** or **2** and TCNQ

possess unconventional segregated−alternated hybrid stack-ings. The results of band structure calculations using the extended Hückel theory support that transfer integrals exist in D−D and D−A stacking columns. Ionicities of the HBCT complexes are ca. 0.4 for **1**·TCNQ and 0.1 for **2**·TCNQ, indicating partial ionic and neutral states, respectively, in agreement with the room-temperature electrical resistivities and activation energies. We believe that HBCT complexes are suitable for subjects of research to create materials showing unique structure and property.

Supporting Information Available: Crystallographic data in CIF format. This material is available free of charge via the Internet at http://pubs.acs.org.

IC0615269

(22) Graja, A. *Low-dimensional Organic Conductors*; World Scientific: Singapore, 1992.

(23) (a) Otwinowski, Z.; Minor, W. *Methods Enzymol.* **1997**, *276*, 307−326. (b) PLATON, Spek, A. L. *J. Appl. Crystallogr.* **2003**, *36*, 7−13.
(24) (a) Sheldrick, G. M. *SHELXS-97 and SHELXL-97*; University of Gottingen: Gottingen, Germany, 1997. (b) Crystal Structure Analysis Package, Molecular Structure Corporation: The Woodlands, TX, 1985 and 1992.
(25) Frisch, M. J.; Trucks, G. W.; Schlegel, H. B.; Scuseria, G. E.; Robb, M. A.; Cheeseman, J. R.; Montgomery, J. A., Jr.; Vreven, T.; Kudin, K. N.; Burant, J. C.; Millam, J. M.; Iyengar, S. S.; Tomasi, J.; Barone, V.; Mennucci, B.; Cossi, M.; Scalmani, G.; Rega, N.; Petersson, G. A.; Nakatsuji, H.; Hada, M.; Ehara, M.; Toyota, K.; Fukuda, R.; Hasegawa, J.; Ishida, M.; Nakajima, T.; Honda, Y.; Kitao, O.; Nakai, H.; Klene, M.; Li, X.; Knox, J. E.; Hratchian, H. P.; Cross, J. B.; Adamo, C.; Jaramillo, J.; Gomperts, R.; Stratmann, R. E.; Yazyev, O.; Austin, A. J.; Cammi, R.; Pomelli, C.; Ochterski, J. W.; Ayala, P. Y.; Morokuma, K.; Voth, G. A.; Salvador, P.; Dannenberg, J. J.; Zakrzewski, G.; Dapprich, S.; Daniels, A. D.; Strain, M. C.; Farkas, O.; Malick, D. K.; Rabuck, A. D.; Raghavachari, K.; Foresman, J. B.; Ortiz, J. V.; Cui, Q.; Baboul, A. G.; Clifford, S.; Cioslowski, J.; Stefanov, B. B.; Liu, G.; Liashenko, A.; Piskorz, P.; Komaromi, I.; Martin, R. L.; Fox, D. J.; Keith, T.; Al-Laham, M. A.; Peng, C. Y.; Nanayakkara, A.; Challacombe, M.; Gill, P. M. W.; Johnson, B.; Chen, W.; Wong, M. W.; Gonzalez, C.; Pople, J. A. *Gaussian 03*, Revision C.01; Gaussian, Inc.: Pittsburgh, PA, 2003.